

Equation-Free Particle-Based Computations: Coarse Projective Integration and Coarse Dynamic Renormalization in 2D

Yu Zou,* Ioannis G. Kevrekidis,[†] and Roger G. Ghanem[‡]

Department of Chemical Engineering and PACM, Princeton University, Princeton, NJ 08544

Department of Civil Engineering, The University of Southern California, Los Angeles, CA 90089

Equation-free approaches have been proposed in recent years for the computational study of multiscale phenomena in engineering problems where evolution equations for the coarse-grained, system-level behavior are not explicitly available. In this paper we study the dynamics of a diffusive particle system in a laminar shear flow, described by a two-dimensional Brownian motion; in particular, we perform coarse projective integration and demonstrate the particle-based computation of coarse self-similar and asymptotically self-similar solutions for this problem. We use marginal and conditional Inverse Cumulative Distribution Functions (ICDFs) as the macroscopic observables of the evolving particle distribution.

Keywords: Equation-free, Coarse projective integration, Coarse dynamic renormalization, Inverse cumulative distribution function, Self-similar, Particle dynamics

1. Introduction

Multiscale phenomena arise naturally in science and engineering. The ability to properly resolve such phenomena and propagate their influence across scales underpins the predictive value of mathematical and physics-based models. In the case of multiscale systems for whose macroscopic behavior no explicit coarse-grained, macroscopic equations are available, a computer-assisted approach, referred to as the *Equation-Free Framework*^{1,2} has been recently proposed. Equation-free methods numerically evolve the coarse-scale behavior through appropriately designed short computational experiments performed by the fine-scale (microscopic, stochastic, agent-based) models. In this paper we will demonstrate the use of two such methods: Coarse Projective Integration (CPI) and Coarse Dynamic Renormalization (CDR).

Particle-based simulators are the fine-scale description of choice for a variety of problems exhibiting multiscale behavior; such problems range from Stokesian and Brownian dynamics to the Monte Carlo modeling of microorganism locomotion, the mixing of passive scalars by turbulent velocity fields and even particle filtering applications. The purpose of Coarse Projective Integration is to accelerate the computational evolution of coarse-grained observables of microscopic simulators; it has been successfully used in the past to accelerate computations of the collective evolution of *spatially one-dimensional* random particle distributions^{3,4}. In those examples, the first motivated by hydrodynamics and the second by bacterial chemotaxis, the coarse-scale observable was the cumu-

lative distribution function (CDF) of the particle positions, synthesized from snapshots of the fine-scale simulation. For one-dimensional problems in space, the functional inverse of the CDF (ICDF) is projected onto a suitable basis set consisting of orthonormal polynomials³ or POD (Proper Orthogonal Decomposition) modes (obtained through Singular Value Decomposition (SVD) of the sorted particle positions⁴). The particle-level model is used to evolve the ICDF, and short time series of the coefficients of its projection on the appropriate basis are thus collected; these short time series are used to estimate the time derivatives of the coefficient evolution. These estimates are then used in the context of traditional continuum integration algorithms (such as Euler⁵, or Adams-Bashforth⁶) to “project” the coefficients forward in time, into the future (thus the term “projective integration”). To repeat the procedure, a “lifting” step is required: fine-scale states, i.e., particle positions whose ICDF is consistent with the projected coefficient values, are generated. Since detailed microscopic evolution over the duration of the projective step has been avoided, the procedure has the potential to alleviate the burden of full fine-scale simulation. Preliminary discussions on the stability and accuracy of these schemes can be found in^{5,7}.

Beyond CPI, equation-free computational protocols can also be used in coarse-grained fixed point and bifurcation analyses, to compute stationary states of the coarse-grained system dynamics and their parametric dependence. In these analyses, the action of operators on the coarse-grained observables is deduced from appropriately initialized computational experiments with the fine scale models. Matrix-free implementations of contraction mappings, like Newton’s method, have been used to compute fixed points of unavailable coarse-scale models for kinetic Monte Carlo (e.g.,⁸, epidemiology), Brownian dynamics⁹ or Lattice Boltzmann^{5,10} fine-scale simulators. The same approach can be used to evolve effective medium (homogenized) descriptions of reaction-transport problems^{11,12} based on *short bursts* of finely resolved simulation.

*Department of Chemical Engineering and PACM, Princeton University.

[†]To whom correspondence should be addressed. Tel.: 1-609-258-2818. E-mail: yannis@princeton.edu. Department of Chemical Engineering and PACM, Princeton University.

[‡]Department of Civil Engineering, The University of Southern California.

For multiscale systems exhibiting *scale invariance* at the macroscopic level, renormalization techniques can be used to solve for self-similar solutions and their scalings¹³, see also^{14,15}. Recently, *dynamic* renormalization (e.g.,^{16,17,18}) was used in conjunction with equation-free computation to obtain coarse-grained self-similar solutions using short bursts of fine-level, direct simulation¹⁹. This *coarse dynamic renormalization* (CDR) method finds macroscopically self-similar solutions with the help of *template functions*^{20,21,22,23}. Observing the macroscopic solutions in a co-expanding (or co-collapsing) frame of reference, we seek *steady states* in the new frame; fixed point equation-free algorithms can be used for this task.

Studying the evolution of particle distributions using their ICDF as an observable is convenient for one-dimensional problems in space, where suitable bases for representing one-dimensional monotonic curves over finite one-dimensional domains are readily available (see the examples in^{3,4,19}). The extension to corresponding observables in more than one dimension, however, is non-trivial: the CDF itself, not being a bijective mapping, does not have an inverse. In this case, operations on the CDF may be implemented by identifying a suitable set of basis functions for two or three-dimensional CDFs. This requires finding multidimensional orthonormal polynomial approximations for monotonic bounded functions with infinite support. In this paper we use an alternative approach, representing a multidimensional CDF in terms of its marginal and one-dimensional conditional distributions. In this manner, multidimensional problems are converted into a collection of one-dimensional problems the solution of which can be obtained using standard approaches. Equation-free algorithms such as CPI and CDR can thus readily be extended to problems involving multidimensional coarse-grained observables. Preliminary results for the self-similar case have been reported elsewhere²⁴.

The paper is organized as follows: In Section 2 a coarse time-stepper is constructed in terms of the marginal and conditional ICDFs in multidimensional particle systems. Use of this time-stepper in CPI and CDR is formulated in Sections 3 and 4, respectively. Our illustrative Brownian particle system in a Couette flow is described in Section 5, and its analytical self-similar and asymptotically self-similar solutions are presented. These two cases are then used in Section 6 to illustrate equation-free computational procedures, and the direct, particle-based computational results are compared with the analytical solutions. We conclude with a brief summary and discussion in Section 7.

2. A Coarse Time-Stepper for Multidimensional Random Particle Systems

Short computational experiments with the fine-scale model are used to construct the coarse time-stepper – the basic element for exchanging dynamical information

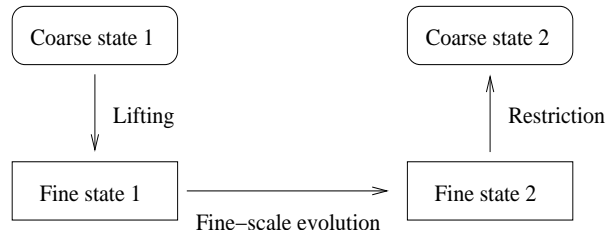


FIG. 1: A schematic of the coarse time-stepper.

between coarse-scale model states and fine-scale states. A coarse time-stepper consists of three components: *lifting*, *fine-scale evolution* and *restriction*⁵ (Fig. 1). The lifting transformation converts coarse-scale observables to consistent fine-scale states; restriction is the reverse transformation, from fine-scale states to coarse-grained observables. Lifting, followed by restriction, should then give the identity on the coarse observables (modulo round-off error). Different coarse time-steppers are generated via different lifting and restriction operators; one should test on-line that macroscopic computational results are insensitive to the specific details of the time-stepper implementation; a more extensive discussion can be found in¹.

For many multiscale problems observed along a single effective spatial dimension, particle positions constitute the fine-scale model state, while an obvious coarse-grained state is the local mean concentration of the particles²⁵. For identical particles this local mean concentration is observed in terms of the histogram of the single particle position probability density function (PDF). However, this PDF histogram depends on the bin size used to estimate it; the PDF at any given point becomes zero if the bin size is too small so that no particles exist within the bin containing this point. To overcome this difficulty, the cumulative distribution function (CDF) is naturally used as an alternative coarse-scale observable. The CDF has in principle infinite support, but its inverse, the Inverse CDF (ICDF), is supported in $[0, 1]$; it can be readily represented by its projection on shifted Legendre polynomials²⁶.

In multidimensional random particle systems, the inverse form of the multidimensional CDF is not readily available (strictly speaking, it is not even defined). The marginal and conditional ICDFs constitute candidate coarse-scale observables for multidimensional systems; this is because the multidimensional CDF can be represented using the marginal CDF in one direction and a collection of conditional CDFs in the remaining directions. For instance, for systems in two spatial dimensions,

$$F_{XY}(x, y) = \int_{-\infty}^y F_{X|Y}(x|y) \frac{dF_Y}{dy}(y) dy, \quad (1)$$

where $F_{XY}(x, y)$, $F_Y(y)$ and $F_{X|Y}(x|y)$ are the CDF, differentiable marginal CDF and conditional CDFs, respectively. The conditional CDF $F_{X|Y}(x|y)$ is defined by

$$\begin{aligned}
F_{X|Y}(x|y) &= \lim_{\Delta y \rightarrow 0} P(X \leq x | y < Y \leq y + \Delta y) \\
&= \lim_{\Delta y \rightarrow 0} \frac{F_{XY}(x, y + \Delta y) - F_{XY}(x, y)}{F_Y(y + \Delta y) - F_Y(y)}. \quad (2)
\end{aligned}$$

Assuming smoothness, a finite number of conditional CDFs can be used to recover the particle distribution (e.g. through interpolation). In the following, we illustrate through a two-dimensional system (without loss of generality) our implementation of this procedure for multidimensional systems.

2.1. Lifting. Starting with the inverse CDFs (ICDF) for the marginal and conditional distributions, the lifting procedure involves obtaining compatible realizations of the fine-scale states. Let the marginal ICDF in direction y , $IF_Y(\cdot) : [0, 1] \mapsto \mathbb{R}$, and conditional ICDFs in the other direction x , $IF_{X|Y}(\cdot, y) : [0, 1] \mapsto \mathbb{R}$, $y \in \mathbb{R}$, be defined by

$$\begin{aligned}
IF_Y(f) &= \arg_{y \in \mathbb{R}} \{F_Y(y) = f\}, \quad f \in [0, 1], \\
IF_{X|Y}(f, y) &= \arg_{x \in \mathbb{R}} \{F_{X|Y}(x|y) = f\}, \quad f \in [0, 1]. \quad (3)
\end{aligned}$$

First, the y -direction position of the i^{th} particle is directly taken from the marginal ICDF as $y_i^s = IF_Y((i - 0.5)/N)$, $i = 1, 2, \dots, N$,³ where N is the number of particles and the superscript s indicates that y_i^s is a sorted, monotonically ascending sequence. Then, corresponding to each y_i^s generated in this manner, the x -direction position of the i^{th} particle is determined as $x_i = IF_{X|Y}(U_i, y_i^s)$, where U_i are i.i.d. real random variables with uniform distribution over $[0, 1]$. We only have a finite number of conditional CDFs, and we will assume that they are smooth in y ; therefore, for each particular working y_i^s we employ the conditional CDFs available in its neighborhood (e.g. the closest one, or possibly an interpolation of the closest ones). Only a few conditional ICDFs are needed if the CDF is sufficiently smooth. For example, if M ($M \ll N$) conditional ICDFs are needed, then these ICDFs, $IF_{X|Y}(f, y_k^c)$, $k = 1, 2, \dots, M$, $f \in [0, 1]$, can be chosen such that $y_k^c = y_{(k-1) \cdot \text{int}(N/M) + \text{int}(N/2M)}^s$, where $\text{int}(\xi)$, $\xi \in \mathbb{R}$ is the maximum integer not greater than ξ .

2.2. Fine-Scale Evolution. We work with multiscale dynamical systems for which we have *fine-scale* evolution models available. For noninteracting particles, letting $\mathbf{X}(t) = (x(t), y(t))^T \in \mathbb{R}^2$ denote the fine-scale model state, consisting of particle positions at time t , the discrete dynamics for \mathbf{X} are given by

$$\mathbf{X}_{k+1} = \Psi(\mathbf{X}_k, \boldsymbol{\eta}_k; \Delta t; \lambda), \quad k = 0, 1, \dots \quad (4)$$

where $\boldsymbol{\eta}_k \in \mathbb{R}^2$ denotes an external stochastic driving force and λ is a set of (constant) parameters. In the class of problems envisioned here, the models $\Psi(\cdot)$ involve microscale simulators of Brownian motion, kinetic Monte Carlo simulation or molecular dynamics.

2.3. Restriction. Let the position of the i^{th} particle be denoted as (x_i, y_i) , $i = 1, 2, \dots, N$ and the sorted

particle positions in two directions be denoted as $\{x_j^s\}$ and $\{y_m^s\}$, respectively. Then a two-dimensional mesh can be formed with each grid point having a coordinate (x_j^s, y_m^s) , $j, m = 1, 2, \dots, N$. For each point (x_j^s, y_m^s) , the number, N_f , of particles whose x and y direction positions satisfy $x_i \leq x_j^s$ and $y_i \leq y_m^s$, respectively, is counted and the CDF at this grid point evaluated as $F_{XY}(x_j^s, y_m^s) = \frac{N_f - 0.5}{N}$. The CDF of particle positions can thus be obtained. This is only one of several possible restriction methods; other restriction approaches can be found in²⁷.

Assuming the CDF $F_{XY}(x, y)$ to be differentiable, Eqn. (1) or (2) lead to the following formula for the conditional CDF,

$$F_{X|Y}(x|y) = \frac{\frac{\partial F_{XY}}{\partial y}(x, y)}{\frac{dF_Y}{dy}(y)}. \quad (5)$$

Continuing the example at the end of Section 2.1, the evaluation of the conditional ICDFs, $IF_{X|Y}(f, y_k^c)$, $k = 1, 2, \dots, M$, $f \in [0, 1]$, requires the availability of the conditional CDFs, $F_{X|Y}(x|y_k^c)$. These can be numerically approximated from equation (5) as,

$$F_{X|Y}(x_j^s | y_k^c) = \frac{F_{XY}(x_j^s, y_{p_2}^s) - F_{XY}(x_j^s, y_{p_1}^s)}{F_{XY}(x_N^s, y_{p_2}^s) - F_{XY}(x_N^s, y_{p_1}^s)}, \quad (6)$$

where p_1 and p_2 can be chosen as $(k - 1) \cdot \text{int}(N/M) + 1$ and $k \cdot \text{int}(N/M)$, respectively. Once the conditional CDF $F_{X|Y}(x|y_k^c)$ is available numerically, the conditional ICDF $IF_{X|Y}(f, y_k^c)$ can be numerically evaluated as in the case of one-dimensional observables.

3. Coarse Projective Integration (CPI) for Multidimensional Random Particle Systems

Coarse projective integrators (CPI) typically consist of four steps (Fig. 2). At first, coarse observables are identified to which the fine-scale model states are restricted. The coarse observables used in our context consist of the marginal and (finitely many) conditional ICDFs of the microscale particle positions, as described in the previous section; in particular, we use a finite number of expansion coefficients (in some appropriate basis) of this marginal and these conditional ICDFs. The particle positions can be generated through the *lifting* procedure described in Section 2.1 once an initial condition for these ICDFs have been specified. We represent the *lifting* operator by μ , a mapping from the coarse observables IF (ICDFs) to the microscopic descriptors \mathbf{X} (particle positions). The second and third steps are the fine-scale evolution and restriction mentioned in sections 2.2 and 2.3, respectively. The restriction operator \mathcal{M} is a mapping from the microscopic descriptors \mathbf{X} to the coarse observables IF , i.e., $IF = \mathcal{M}\mathbf{X}$. Evidently, the operators \mathcal{M} and μ satisfy the property $\mathcal{M}\mu = I$ (modulo roundoff error). Along with restriction comes the estimation of

the coarse-scale time derivatives of the observables (the marginal and ICDF coefficients).

The last step is the projection step in time – the temporal evolution of our representation of the coarse-scale observables. This step is templated on continuum numerical integration techniques - for coarse forward Euler it is simple linear extrapolation of the coarse observables in time, although more sophisticated and even implicit techniques can be (and have been) used^{5,28}.

Let the coarse-scale observables at time t consist of $M + 1$ ICDFs, $IF_{i,t}, i = 1, \dots, M + 1$, of which the first one is the marginal ICDF, $IF_Y(f)$, and the remaining ones are the conditional CDFs, $IF_{X|Y}(f, y_k^c)$, at y -direction positions $y_k^c, k = 1, 2, \dots, M$. Let a basis of the coarse-scale subspace, which can be specified globally^{3,4} or locally⁴, be denoted by $\{\theta_q\}$. Then the projections, $\beta_{i,q,t}$, of ICDFs onto the basis can be computed by,

$$\beta_{i,q,t} = (IF_{i,t}, \theta_q), \quad q = 0, 1, \dots, P \quad t = 1, 2, \dots, n, \quad (7)$$

where the inner product is in L_2 .

The projective integration step over a coarse-scale time step T can be formally written as

$$\beta_{i,q,n+T} = L(\beta_{i,q,l+1}, \beta_{i,q,l+2}, \dots, \beta_{i,q,n}), \quad (8)$$

where $L(\cdot)$ is an operator based on (templated on) traditional continuum numerical integration schemes, $\beta_{i,q,n+T}$ is the coefficient of the q^{th} mode of the i^{th} ICDF immediately after the temporal projection step and $\beta_{i,q,t}, t = l + 1, \dots, n$ is the coefficient of the q^{th} mode corresponding to the t^{th} fine-scale time step prior to the projective step.

Immediately after the projective sep, the new ICDFs, $IF_{i,n+T}$, based on the new coefficients $\beta_{i,q,n+T}$, are constructed as,

$$IF_{i,n+T} = \sum_{q=0}^P \beta_{i,q,n+T} \theta_q \quad (9)$$

New fine-scale model states can then be “lifted” from the ICDFs, $IF_{i,n+T}$.

Using the above steps, the procedure for applying CPI to multidimensional random particle systems can be summarized as follows:

1. Generate fine-scale model state(s) consistent with the coarse-scale description given by the particle ICDFs. The marginal and conditional ICDFs can be obtained through equation (5) if an analytical two-dimensional CDF is given as the initial condition.

2. Let the fine-scale model state evolve according to the discrete dynamical model (4)

3. Generate ICDFs at some successive fine-scale time steps.
4. Project the ICDFs onto an appropriate basis (equation (7)), and estimate the temporal derivatives of coefficients of the dominant modes.
5. Extrapolate (project forward in time) coefficients of the dominant modes over a large coarse-scale time interval T (equation (8)), reconstruct the ICDFs (equation (9)) and go back to step 1.

Usually one wants to report the multidimensional CDFs, and they can be generated numerically along with the ICDFs using the approach in Section 2.3 (although only the ICDFs are taken as coarse-scale states involved in the CPI method). The mesh size for numerically computing the CDF can be set larger than $\max_{1 \leq i \leq N-1} (x_{i+1}^s - x_i^s, y_{i+1}^s - y_i^s)$, in an attempt to alleviate fluctuation-related problems in the estimation step; variance reduction schemes (multiple realizations of the simulation, or more sophisticated approaches) may become necessary for this purpose.

4. Coarse Dynamic Renormalization (CDR) for Multidimensional Random Particle Systems

For multiscale systems of practical interest, if the PDEs in the macroscopic level are scale invariant, they may possibly possess self-similar solutions¹³. The analogy with traveling wave solutions for problems with translational invariance is instructive: approaching a traveling wave in a co-traveling frame appears like the approach to a stationary state. Similarly, approaching a self-similar solution in a dynamically renormalized (co-exploding or co-collapsing) frame, appears like the approach to a stationary state. Dynamic renormalization procedures have been used to investigate self-similar systems^{16,17,18}; recently a template-based approach for studying the dynamics of problems with translational symmetry²⁰ has been extended to study the dynamics of problems with scale invariance^{19,21,22,23}. When macroscopic scale-invariant PDEs are explicitly available, template conditions can be used to derive dynamical equations (termed “MN-dynamics”) for the rescaled self-similar solutions and similarity exponents²¹. The idea of employing template conditions can also be used to obtain renormalized self-similar macroscale solutions and similarity exponents for multiscale systems whose coarse-level PDEs are not explicitly known¹⁹. The number of template conditions depends on how many rescaling variables are needed to renormalize the physical solutions.

Consider a PDE in the form of

$$\frac{\partial F}{\partial t} = D_{xy}(F), \quad (10)$$

where $F(x, y, t)$ is a CDF of particle positions which do not collectively translate in the space domain (the case of

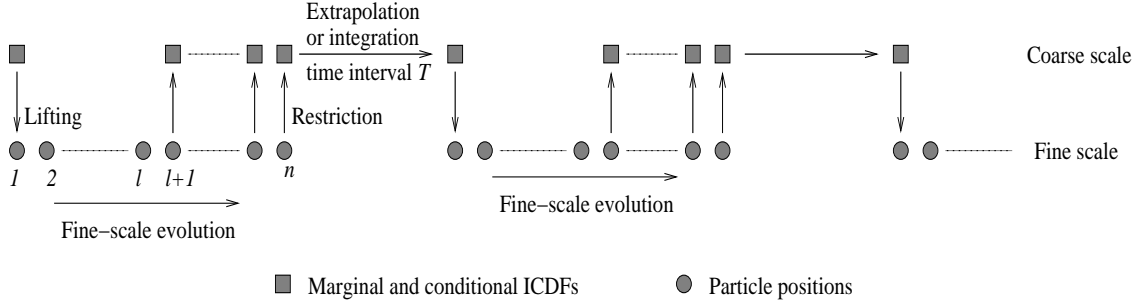


FIG. 2: The evolution of the coarse and fine-scale model states.

joint scale and translational invariance can also be simply treated, see²³).

The differential operator D_{xy} is such that there exist constants p and a such that

$$D_{xy}(f(\frac{x}{A}, \frac{y}{A^p})) = A^a D_{uv}(f(u, v)), \quad u = \frac{x}{A}, \quad v = \frac{y}{A^p}, \quad (11)$$

for any real function f , real value $A > 0$ and coordinate (x, y) (there is no amplitude rescaling since this is a CDF). If a self-similar solution $F(x, y, t)$ exists, it can be written as

$$F(x, y, t) = U(\frac{x}{(cs)^\alpha}, \frac{y}{(cs)^{\alpha p}}; c), \quad (12)$$

where c is a constant parametrizing the family of self-similar shapes, $s = t - t_0$, (t_0 is the blowup time for problems with finite time singularities) and $t > t_0$. Substituting (12) into (10), we have

$$\alpha a = -1, \quad (13)$$

and U satisfies the PDE,

$$-\alpha u U_u - \alpha p v U_v = c^{-1} D_{uv}(U), \quad (14)$$

where $u = x/(cs)^\alpha$, $v = y/(cs)^{\alpha p}$. For the operator D_{xy} that satisfies Eqn. (11), the constant a is determined by D_{xy} itself. Hence the similarity exponent α can be calculated by Eqn.(13).

If the macroscopic equation (10) is not explicitly known, one cannot analytically obtain the exponents p and a ; numerical computations are needed to determine these constants – and thus to test the scale invariance of the operator – before locating the self-similar solutions themselves. For an operator D_{xy} that satisfies the (unknown) equation (11), the constants p and a can be obtained using a black box simulator of the equation as follows: Since the unknown Eqn. (11) is valid for *any* coordinate (x, y) and real function f , let f be a test function (we choose it here for convenience to be exponential in space) $(x_1, y_1) = (u_1, A v_1, A^p)$ and

$(x_2, y_2) = (u_2 A, v_2 A^p)$, where A is arbitrarily chosen as a positive real value. This would imply that (choosing two points in space) the following two relations hold:

$$D_{xy}(f(\frac{x}{A}, \frac{y}{A^p}))(x_1, y_1) = A^a D_{uv}(f(u, v))(u_1, v_1),$$

$$D_{xy}(f(\frac{x}{A}, \frac{y}{A^p}))(x_2, y_2) = A^a D_{uv}(f(u, v))(u_2, v_2),$$

where (u_1, v_1) and (u_2, v_2) are two distinct coordinates. Comparing the above two equations, we have

$$\frac{D_{xy}(f(\frac{x}{A}, \frac{y}{A^p}))(x_1, y_1)}{D_{xy}(f(\frac{x}{A}, \frac{y}{A^p}))(x_2, y_2)} = \frac{D_{uv}(f(u, v))(u_1, v_1)}{D_{uv}(f(u, v))(u_2, v_2)}. \quad (15)$$

Therefore, the constant p is the solution to Eqn. (15). We rewrite Eqn.(15) as

$$D_{xy}(f(\frac{x}{A}, \frac{y}{A^p}))(x_2, y_2) - \frac{D_{xy}(f(\frac{x}{A}, \frac{y}{A^p}))(x_1, y_1)}{D_{uv}(f(u, v))(u_1, v_1)} D_{uv}(f(u, v))(u_2, v_2) = 0. \quad (16)$$

The constant p can then be solved for, employing an in principle arbitrary test function f , and using Newton's method. Since we assumed that the operator D_{xy} is not explicitly available, $D_{xy}(f(x, y))$ can be estimated by running the micro-simulator for short time “bursts” and numerically obtaining the derivative $\frac{\partial f}{\partial t}$. The constant a is calculated by

$$a = \log_A \frac{D_{xy}(f(\frac{x}{A}, \frac{y}{A^p}))(x_1, y_1)}{D_{uv}(f(u, v))(u_1, v_1)}, \quad (17)$$

once p is obtained. Clearly, other test functions and conditions evaluated at other points can be used; care must be taken also to ensure the finiteness of the estimated quantities.

Given p , to determine the self-similar shape of the solution, we consider the general scaling

$$F(x, y, t) = \omega(\frac{x}{A(t)}, \frac{y}{A(t)^p}, t), \quad (18)$$

where $A(t)$ is an unknown function. The PDE becomes

$$\omega_t - \frac{A_t}{A} u \omega_u - \frac{p A_t}{A} v \omega_v = A^a D_{uv}(\omega). \quad (19)$$

Evidently, U and ω are both renormalized CDFs.

By comparing equations (14) and (19), we have

$$\alpha = \frac{\lim_{t \rightarrow \infty} \frac{A_t}{A}}{\lim_{t \rightarrow \infty} cA^\alpha}. \quad (20)$$

Also by comparing equations (12) and (18), we have

$$\frac{\lim_{t \rightarrow \infty} A}{\lim_{t \rightarrow \infty} (cs)^\alpha} = 1. \quad (21)$$

The above equations (20) and (21) together with (13) lead to

$$\alpha = \lim_{t \rightarrow \infty} \frac{(t - t_0)A_t}{A}. \quad (22)$$

Therefore, the value for α can be calculated once values of $A(t)$ are obtained in the long-time limit (i.e., after ω reaches the steady state). Indeed, let t_1 and t_2 be distinct times after ω reaches the steady state, then by (22),

$$\alpha = \frac{t_2 - t_1}{\frac{A(t_2)}{A_t(t_2)} - \frac{A(t_1)}{A_t(t_1)}}. \quad (23)$$

A single template condition is required to solve for both $\omega(u, v, t)$ and $A(t)$ at every time step. In this paper, the template is chosen to be

$$\omega(e, \infty, t) = m, \quad e < 0, \quad 0 < m < 0.5, \quad (24)$$

where e and m are both constants. The template condition has the following physical meaning: the rescaled marginal CDF ω_U always has the same value m at the u-direction coordinate e for all time t . Applying this template to Eqn.(19) and assuming $\frac{\partial \omega}{\partial v}(e, v, t)$ decays exponentially as $v \rightarrow \infty$, we have

$$A_t e \frac{\partial \omega}{\partial u}(e, \infty, t) + A^{a+1} D_{uv}(\omega)(e, \infty, t) = 0. \quad (25)$$

Equations (19) and (25) can be coupled to solve for the rescaled CDF ω and rescaling variable A if the operator D_{xy} is explicitly known. As the time $t \rightarrow \infty$, ω may approach a steady state, which is then a stable self-similar shape for the solutions to Eqn.(10). In general cases, the macroscale equation for the CDF of the particle positions may not be explicitly available. However, the template-based approach can still be used to renormalize the CDF evolved via microscale models and rescaling variables are obtained during the course of renormalization. In these cases, to express the CDFs, the marginal and conditional ICDFs are used again as macroscopic observables, and their (discretized) projections over an orthonormal basis are again used to numerically characterize them through a finite number of coefficients. Based on the coarse time-stepper, the procedure for the coarse renormalization is schematically depicted in Fig. 3 and consists of the following steps

1. Generate the marginal and conditional ICDFs $IF_{i,t}, i = 1, \dots, M+1$ according to the initial CDF using equation (5) or (6) or according to the coefficients, $\beta_{i,q,t}$, of dominant modes of the ICDFs using equation (9).
2. Generate particle positions using the ICDFs using the *lifting* procedure in the coarse time-stepper.
3. Evolve particle positions over a time interval T' using a fine-scale model (4).
4. Obtain ICDFs from particle positions using the *restriction* procedure in the coarse time-stepper.
5. Rescale the marginal ICDF according to the template condition and obtain the rescaling variable A . We then rescale the conditional ICDFs by a factor of A^p . This step can be justified by Eqn.(18). Indeed, obtaining the rescaled solution ω_{k+1} from ω_k via the dynamics (19) and (25) is equivalent to starting from the initial condition ω_k , running the original dynamics for a while to get F_{k+1} , factoring out the rescaling variable A , and rescaling F_{k+1} in scales of A and A^p respectively in x and y directions.
6. Project the rescaled ICDFs onto the orthonormal basis and obtain the coefficients of leading modes using equation (7). Go back to step 2.

The above procedure can be viewed as an iterative algorithm to solve the fixed point of a nonlinear operator $\Phi_{T'}$, written as,

$$\beta = \Phi_{T'}(\beta). \quad (26)$$

This fixed point can be written in component form as, $\beta_{i,q}^r, i = 1, \dots, M+1, q = 0, \dots, P$,¹⁹ or

$$\beta = (\beta_{1,0}^r, \beta_{1,1}^r, \dots, \beta_{1,P}^r, \beta_{2,0}^r, \beta_{2,1}^r, \dots, \beta_{2,P}^r, \dots, \beta_{M+1,0}^r, \beta_{M+1,1}^r, \dots, \beta_{M+1,P}^r)^T,$$

where the superscript r refers to the fact that this is the renormalized self-similar shape. These coefficients correspond to the renormalized self-similar ICDFs and CDF of the multidimensional particle system. Equation (26) may be solved using any numerical algorithm such as direct iteration or matrix-free (Krylov-subspace based) implementations of Newton's method²⁹.

5. Self-Similar and Asymptotically Self-Similar Dynamics of Brownian Particles in a Couette Flow

We will use CPI and CDR algorithms to study two-dimensional Brownian models of particle dispersion in a Couette flow³⁰. In this section, a particle system with self-similar dynamic evolution and a system with asymptotically self-similar evolution are explored, respectively

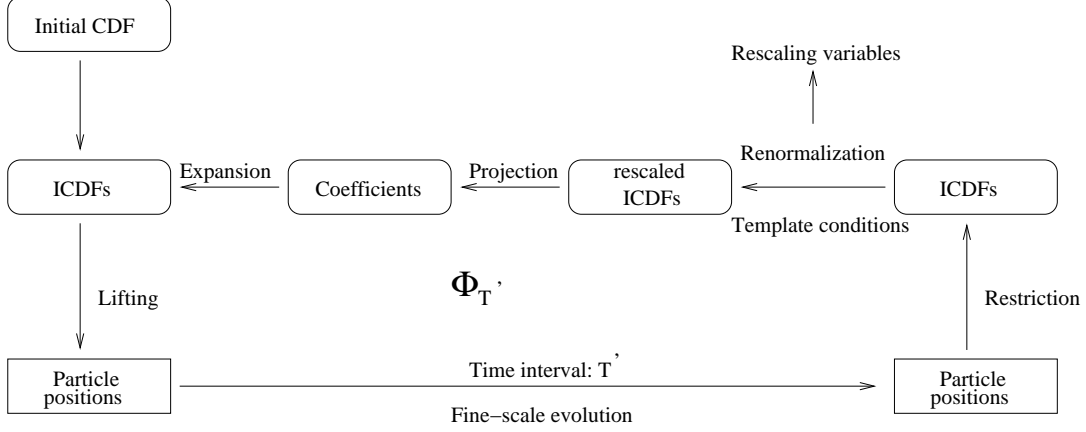


FIG. 3: Schematic illustration of coarse dynamic renormalization.

5.1. A Particle System with Self-Similar Dynamics. Let $X(t)$ and $Y(t)$ represent particle positions in x and y directions respectively at time t on an infinite two-dimensional spatial domain. The particle positions in the two directions evolve in this model governed by the following dynamics:

$$dX(t) = DdW_X(t), \quad dY(t) = Xdt, \quad (27)$$

where $W_X(t)$ is a Wiener processes³¹ and D is the diffusion coefficient. The discretized dynamics of (27) is given by³²

$$X_{k+1} = X_k + D\eta_{X,k}\sqrt{\Delta t}, \quad Y_{k+1} = Y_k + X_k\Delta t, \quad (28)$$

where $\eta_{X,k}$ are i.i.d. standard Gaussian random variables.

The dynamics (27) represent the motion of particles which only diffuse in the x -direction in a Couette flow. It can be shown that the coarse-scale dynamics for the PDF, $P_{XY}(x, y, t)$, of a particle position, corresponding to the fine-scale dynamics (27), is governed by the following equation²⁵

$$\frac{\partial P_{XY}}{\partial t} + x \frac{\partial P_{XY}}{\partial y} = \frac{D^2}{2} \frac{\partial^2 P_{XY}}{\partial x^2}, \quad (29)$$

where P_{XY} is assumed to be 2nd-order differentiable. Hence the dynamics for the CDF, $F_{XY}(x, y, t)$, associated with (29) is given by

$$\frac{\partial F_{XY}}{\partial t} + x \frac{\partial F_{XY}}{\partial y} - \int_{-\infty}^x \frac{\partial F_{XY}}{\partial y} dx = \frac{D^2}{2} \frac{\partial^2 F_{XY}}{\partial x^2}. \quad (30)$$

In the above equation, the operator D_{xy} is written as

$$D_{xy} = -x \frac{\partial}{\partial y} + \int_{-\infty}^x \frac{\partial}{\partial y} dx + \frac{D^2}{2} \frac{\partial^2}{\partial x^2}. \quad (31)$$

This operator satisfies the scale invariance property (11) for constant values $p = 3$ and $a = -2$. The analytical self-similar solution to Eqn. (29) is inspired by³³

(See Appendix A)

$$P_{XY}(x, y, t) = \frac{\sqrt{3}}{\pi D^2 (t - t_0)^2} e^{-\left(\frac{6(y - 0.5x(t - t_0))^2}{D^2(t - t_0)^3} + \frac{x^2}{2D^2(t - t_0)}\right)}, \quad (32)$$

where t_0 is the blowup time (backward in time), which then gives the self-similar solution to (30),

$$F_{XY}(x, y, t) = \frac{\sqrt{3}}{\pi D^2 (t - t_0)^2} \int_{-\infty}^x \int_{-\infty}^y e^{-\left(\frac{6(y - 0.5x(t - t_0))^2}{D^2(t - t_0)^3} + \frac{x^2}{2D^2(t - t_0)}\right)} dy dx. \quad (33)$$

Let $u' = \frac{x}{(c(t - t_0))^{1/2}}$ and $v' = \frac{y}{(c(t - t_0))^{3/2}}$, then

$$F_{XY}(x, y, t) = F_{UV}(u', v') = \frac{\sqrt{3}}{\pi D^2 / c^2} \int_{-\infty}^{u'} \int_{-\infty}^{v'} e^{-\left(\frac{6(v' - 0.5u'/c)^2}{D^2/c^3} + \frac{u'^2}{2D^2/c}\right)} dv' du'. \quad (34)$$

Hence for the integro-differential equation (30), the similarity exponent in (12) is $\alpha = 1/2$. For the CDF in (34), its standard deviations (std.'s) in two directions and correlation are $\sigma_X = D/c^{1/2}$, $\sigma_Y = D/(\sqrt{3}c^{3/2})$, and $\rho_{XY} = \sqrt{3}/2$, respectively.

5.2. A Particle System with Asymptotically Self-Similar Dynamics. We now consider Brownian particles in a Couette flow that diffuse in both spatial directions. The microscopic-level evolution equation for the particle positions is given by

$$dX(t) = DdW_X(t), \quad dY(t) = Xdt + DdW_Y(t), \quad (35)$$

where $W_X(t)$ and $W_Y(t)$ are independent Wiener processes. The discretized dynamics of (35) are given by³²

$$\begin{aligned} X_{k+1} &= X_k + D\eta_{X,k}\sqrt{\Delta t}, \\ Y_{k+1} &= Y_k + X_k\Delta t + D\eta_{Y,k}\sqrt{\Delta t} \end{aligned} \quad (36)$$

where $\eta_{X,k}$ and $\eta_{Y,k}$ are i.i.d. standard Gaussian random variables.

The coarse-scale PDF of the particle positions is governed by²⁵

$$\frac{\partial P_{XY}}{\partial t} + x \frac{\partial P_{XY}}{\partial y} = \frac{D^2}{2} \frac{\partial^2 P_{XY}}{\partial x^2} + \frac{D^2}{2} \frac{\partial^2 P_{XY}}{\partial y^2}. \quad (37)$$

Accordingly, the dynamics for the CDF, $F_{XY}(x, y, t)$, are given by

$$\begin{aligned} \frac{\partial F_{XY}}{\partial t} + x \frac{\partial F_{XY}}{\partial y} - \int_{-\infty}^x \frac{\partial F_{XY}}{\partial y} dx \\ = \frac{D^2}{2} \frac{\partial^2 F_{XY}}{\partial x^2} + \frac{D^2}{2} \frac{\partial^2 F_{XY}}{\partial y^2}. \end{aligned} \quad (38)$$

In Eqn. (38), the operator D_{xy} is written as

$$D_{xy} = -x \frac{\partial}{\partial y} + \int_{-\infty}^x \frac{\partial}{\partial y} dx + \frac{D^2}{2} \frac{\partial^2}{\partial x^2} + \frac{D^2}{2} \frac{\partial^2}{\partial y^2}. \quad (39)$$

The above operator does not exactly satisfy the scale invariance property (11) for any function f , positive real value A and coordinate (x, y) . However, as *the scale* of the function f or the value of A become sufficiently large, there may exist p and a such that (11) is *approximately* satisfied. At those limits for f and/or A , values of p and a that approximately satisfy (11) approach the values that exactly satisfy the scale invariance property in the true self-similar case.

The asymptotically self-similar solution to the equation (37) is given by³⁴

$$P_{XY}(x, y, t) = \frac{1}{2\pi D^2 (t - t_0) (1 + (t - t_0)^2 / 12)^{1/2}} e^{-\left(\frac{(y - 0.5x(t - t_0))^2}{2D^2(t - t_0)(1 + (t - t_0)^2 / 12)} + \frac{x^2}{2D^2(t - t_0)}\right)}, \quad (40)$$

which then provides the asymptotically self-similar solution to (38),

$$\begin{aligned} F_{XY}(x, y, t) = \frac{1}{2\pi D^2 (t - t_0) (1 + (t - t_0)^2 / 12)^{1/2}} \\ \int_{-\infty}^x \int_{-\infty}^y e^{-\left(\frac{(y - 0.5x(t - t_0))^2}{2D^2(t - t_0)(1 + (t - t_0)^2 / 12)} + \frac{x^2}{2D^2(t - t_0)}\right)} dy dx. \end{aligned} \quad (41)$$

Let $u' = \frac{x}{(c(t - t_0))^{1/2}}$ and $v' = \frac{y}{(c(t - t_0))^{3/2}}$, then

$$\begin{aligned} F_{XY}(x, y, t) = F_{UV}(u', v', t) = \\ \frac{\sqrt{3}(t - t_0)}{\pi D^2 ((t - t_0)^2 + 12)^{1/2} / c^2} \\ \int_{-\infty}^{u'} \int_{-\infty}^{v'} e^{-\left(\frac{6(v - 0.5u/c)^2 (t - t_0)^2}{D^2((t - t_0)^2 + 12)/c^3} + \frac{u^2}{2D^2/c}\right)} dv du. \end{aligned} \quad (42)$$

In the long-time limit, $F_{UV}(u', v', t)$ has a steady-state form, which is the same as that given by (34) in the self-similar case

6. Numerical Examples

In what follows, direct particle simulations are implemented to accelerate the numerical evolution of the CDFs via CPI, and to locate self-similar CDFs via CDR for the particle systems in Section 5. The approximate (asymptotic) scale invariance of the macroscale differential operator D_{xy} for the asymptotically self-similar particle system is also examined. The fixed-point algorithm in Section 4 is utilized to solve for the long-time steady-state shape of the CDF for the asymptotically self-similar system. The diffusion coefficient D and simulation time step Δt in the fine-scale model are set to $5.0 \text{ cm/s}^{1/2}$ and 0.01 s , respectively. An ensemble of 2000 ($N = 2000$) particles is used in the fine-scale simulations except where otherwise indicated.

Simulation 1: Direct Simulation of the Self-Similar Particle System

In this simulation, the initial fine-scale particle positions are chosen to follow a uniform distribution over the square domain $(-10 \text{ cm}, 10 \text{ cm}) \times (-10 \text{ cm}, 10 \text{ cm})$. An ensemble of 2000 particles whose distribution is consistent with the coarse-scale initial conditions are evolved directly using (28) and used to construct true evolved coarse-scale CDFs. Particle positions are recorded at the time $300\Delta t$, $600\Delta t$ and $900\Delta t$, respectively. Two-dimensional CDFs are numerically computed using the procedure in Section 2.3 and plotted in Fig. 4. The number of grid points used to compute the CDFs is 1681.

Simulation 2: Coarse Projective Integration of the Self-Similar Particle System

We now use CPI to accelerate the evolution of the coarse-scale observables. The coarse-scale initial condition is the same as that in Simulation 1. Particles are evolved for an initial block of 10 ($l = 10$) fine-scale time steps and then again for another block of 10 ($n - l = 10$) fine-scale time steps. At each of the latter 10 steps, the marginal ICDF and 20 ($M = 20$) conditional ICDFs of particle positions are formed; the time series of the coefficients of their leading modes is linearly extrapolated (with a slope estimated through least-squares) over a time interval equal to 10 ($T = 10$) fine-scale time steps. The basis onto which the ICDFs are projected consists here of shifted Legendre polynomials of order up to and including 5 ($P = 5$). Since the ICDFs are anti-symmetric with respect to the axis $f = 0.5$, the coefficients of the 2nd and 4th modes vanish. Hence, only 84 coefficients need to be extrapolated. At the end of the extrapolation, the ICDFs are reconstructed and particle positions, generated according to these ICDFs, are simulated again. At time $300\Delta t$, $600\Delta t$ and $900\Delta t$, particle positions are recorded and CDFs plotted in Fig. 5. The number of grid points used to compute CDFs is again 1681. The cross sections, $F_{XY}(s, s, t)$, of CDFs in Simulation 1 and 2 are compared in Fig. 6, which shows an excellent visual match between the true CDFs and those computed from the CPI algorithm.

No. of Iterations	p	a
0	5.0	-3.34959
1	2.80093	-1.88311
2	2.99246	-2.03967
3	3.00106	-2.04212
4	3.00370	-2.05468
5	2.99592	-2.03927
6	2.99659	-2.03914
7	2.99753	-2.04017
8	2.99831	-2.04189

TABLE I: Iterative evaluation of the constants p and a .

No. of Iterations	p	a
0	5.0	-3.38239
1	3.19621	-2.25167
2	2.97334	-2.06146
3	2.99987	-2.08557
4	2.99574	-2.08444
5	2.99347	-2.08425
6	2.99747	-2.08345
7	2.99247	-2.08073
8	2.99833	-2.08601

TABLE II: Iterative values for the constants p and a for a different set of algorithm parameters (see text).

Simulation 3: Coarse Dynamic Renormalization of the Self-Similar Particle System

Pretending that the macroscale equation (30) is not available, we now directly use the microscale simulator (28) to compute the constants p and a , the similarity exponent α and the macroscopic self-similar solution.

In the approach provided in Section 4, Newton's method is used to solve the equation (17) for p . The test function f was first chosen as a 2-dimensional joint Gaussian distribution function, $f(x, y) = 1/16N(x/4)N(y/4)$, where $N(x)$ and $N(y)$ are standard Gaussian distributions. We select the value of the positive real number $A = 2.0$. The two coordinates (u_1, v_1) and (u_2, v_2) in (17) are chosen as $(-2, -2)$ and $(3, 3)$, respectively. To reduce fluctuations of values for the operator D_{xy} , 9000 particles are used and 500 replica copies of values for D_{xy} and D_{uv} are averaged in the computation.

Starting from the initial value $p_0 = 5.0$, iterative values for p are stabilized at 3.0 after 3 iterations. Accordingly, the converged value for a is -2.0 (Table I).

For verification, we choose another set of parameters to determine p and a : $f(x, y) = 1/25N(x/5)N(y/5)$, $A = 2.5$, $(u_1, v_1) = (-3, -3)$, and $(u_2, v_2) = (4, 4)$. Again, starting from the initial value $p_0 = 5.0$, iterative evaluations of p are stabilize at 3.0 after 3 iterations and the converged value for a is again around -2.0 (Table II).

We can therefore conclude that there exist $p = 3.0$ and $a = -2.0$ such that the unavailable differential operator D_{xy} corresponding to the microsimulator (27) possesses the scale invariance property (11). Accordingly, the similarity exponent is $\alpha = 0.5$ by Eqn. (13)

$t(sec)$	$A(t)$	$A_t(t)$
0	1.00000	-
1	1.10268	0.10268
3	1.27793	0.08763

TABLE III: The rescaling variable $A(t)$.

The template condition for the x direction is chosen to be $\omega(-2.832, \infty, t) = 0.4$, i.e., the u -coordinate corresponding to the renormalized marginal CDF $\omega_U = 0.4$ always has the same value, $-2.832cm$. The constant c in the analytical solution (34) is obtained as $c = 0.2sec^{-1}$ based on our template. The corresponding std.'s for the analytical self-similar shape are $\sigma_X = 5\sqrt{5}cm$ and $\sigma_Y = 25\sqrt{15}/3cm$, respectively.

The CDF corresponding to a uniform distribution of particle positions over the space domain $(-10cm, 10cm) \times (-10cm, 10cm)$ is used as the initial condition. Direct iteration is used to solve for the fixed point of equation (26). The time interval T' is $100\Delta t$. The number of conditional ICDFs is 20 ($M = 20$) and the basis for the ICDFs is again the shifted Legendre polynomials of order up to and including 5 ($P = 5$). In this simulation, 100 copies of ensemble particle positions are generated according to the mode coefficients of the ICDFs at the beginning of each iteration and let to evolve. The mode coefficients at the end of each iteration are obtained by averaging over these 100 replica copies. After the 2nd, 4th and 6th iterations, renormalized mode coefficients of the ICDFs are used to generate particle positions, out of which the CDFs are computed and plotted respectively in Fig. 7. Fig. 8 also compares the cross sections $\omega(u, u, t)$ of true CDFs and renormalized CDFs in this simulation. Clearly, the renormalized solutions quickly approach the self-similar steady state.

To validate the computation of the self-similar solution shape, the std.'s and correlation of the computed shape are compared with those of the known analytical solution. The std.'s and correlations of the rescaled CDFs are calculated via the ensemble particle positions corresponding to these CDFs. The comparison is shown in Fig. 9, where curves in Case 1 represent results obtained using this template condition and time interval. The std.'s and correlations of the rescaled CDFs approach those of the analytical self-similar shape, which means that the rescaled CDF coincides eventually with a member in the family of theoretical self-similar shapes expressed by Equation (34).

As the renormalized CDF ω reaches its steady state, we can set this CDF as the initial condition and evolve the microscale dynamics (28) for two more loops with $t_1 = 100\Delta t$ and $t_2 = 300\Delta t$. The rescaling variable $A(t)$ is listed in Table III. Note that $A(t) = 1$ at $t = 0$. By Equation (23), the similarity exponent α is approximated as 0.520, within 4% of the theoretical value $1/2$.

In the following, the effect of variation of templates and evolution times of the fixed-point operator $\Phi_{T'}$ on

No. of Iterations	p	a
0	5.0	-3.87764
1	4.14589	-3.32940
2	3.81151	-3.09345
3	3.78553	-3.08460
4	3.79408	-3.08433
5	3.78576	-3.08486
6	3.79758	-3.08472
7	3.78701	-3.09319
8	3.79517	-3.08471

TABLE IV: Iteratively computed values of p and a for Parameter set 1 (see text).

the computed renormalized self-similar shapes will be examined. For self-similar systems, we can see from Eqn. (19) that, as the system reaches the steady state, the rescaled shape of CDFs will remain the same, irrespective of changes in the evolution time T' . Also, the steady-state CDF shapes will coincide with members in the family of self-similar solutions prescribed by Eqn. (14) no matter what the scale of the template is.

We choose four cases of the template condition and evolution time including the one above:

1. $\omega(-2.832, \infty, t) = 0.4, T' = 100\Delta t;$
2. $\omega(-2.832, \infty, t) = 0.4, T' = 200\Delta t;$
3. $\omega(-0.283, \infty, t) = 0.4, T' = 100\Delta t;$
4. $\omega(-0.283, \infty, t) = 0.4, T' = 200\Delta t.$

The iterative values of std.'s and correlation for the four cases are shown in figures 9 and 10. Comparison with theoretical calculations shows that variation of templates and evolution times indeed does not cause deviation of the converged rescaled CDF from the family of self-similar solutions.

Simulation 4: Coarse Dynamic Renormalization of the Asymptotically Self-Similar Particle Dynamics

For the particle system in Section 5.2, the procedure in Section 4 is used to check if its macroscopic differential operator D_{xy} possesses the scale invariance property (11). The two parameter sets in Simulation 3 are used here.

1. Parameter set 1: $f(x, y) = 1/16N(x/4)N(y/4), A = 2.0, (u_1, v_1) = (-2, -2), (u_2, v_2) = (3, 3);$
2. Parameter set 2: $f(x, y) = 1/25N(x/5)N(y/5), A = 2.5, (u_1, v_1) = (-3, -3), (u_2, v_2) = (4, 4).$

Newton's method is utilized again to solve for p and a for each parameter set. The iteratively computed values of p and a are listed in tables IV and V.

It can be seen that now converged values of p and a do vary with the template scale and value of A . As

No. of Iterations	p	a
0	5.0	-4.23757
1	4.47814	-3.85506
2	2.58903	-1.95833
3	4.01019	-3.38693
4	3.64906	-2.96049
5	3.35744	-2.69786
6	3.39829	-2.74037
7	3.40776	-2.75770
8	3.41325	-2.74170
9	3.41298	-2.75793

TABLE V: Iteratively computed values of p and a for Parameter set 2 (see text).

the template scale and A increase, values of p and a approach those in the self-similar case. Pretending that the macroscale equation is not explicitly known, we may suspect that the particle system exhibits asymptotically self-similar dynamics. Therefore, for ‘‘asymptotically large enough’’ template conditions, the operator D_{xy} still approximately possesses the scale invariance property (11); as we did in the self-similar case, we can use a fixed point algorithm to find a long-time steady state for the asymptotically self-similar solution. In analogy to the self-similar case, the evolution time interval in the fixed-point operator does not affect the converged shape for such large enough scales.

The four template condition and evolution time cases in Simulation 3 are used in the fixed point algorithm to verify the above assertions. The value p is set to 3.0, the same value as that in Simulation 3. The microsimulator is the discretized dynamics (36). Iterative values of std.'s and correlation for the four cases are shown in figures 11 and 12. As can be seen, for large template conditions, the length of evolution time T' does not affect the converged values of std.'s and correlation for distribution of particle positions. Yet for small templates, the effect of T' on the y -direction std. and correlation is evident. As T' increases from $100\Delta t$ to $200\Delta t$, the converged values of y -direction std. and correlation approach their expected theoretical values.

7. Conclusions and Remarks

We presented an equation-free computational approach, based on using marginal and conditional ICDFs as coarse-scale observables, for the computer-assisted study of multidimensional random particle system dynamics. Coarse projective integration employing this time-stepper can be applied to accelerate the computational evolution of particle CDF computations; the approach targets multidimensional particle systems whose coarse-scale models are not explicitly available. Coarse dynamic renormalization can also be used to analyze particle systems with self-similar or asymptotically self-similar coarse-grained evolution dynamics, and to obtain long-time renormalized steady state (self-similar) solu-

tions.

The examples in this paper are admittedly simple, yet they illustrate the computational approaches in a context where the results can be validated; we hope that the type of multiscale algorithms presented here may be useful in more complicated situations (e.g., particles mixing in time-dependent velocity fields) if the macroscopic dynamic are effectively self-similar. Another possible application of such equation-free approaches is in cases where even *the coarse-scale observables* are characterized by uncertainty/stochasticity. Polynomial chaos observables have been used in the solution of explicit macroscale PDEs for passive scalar transport, where the uncertainty enters through random initial conditions or boundary conditions^{35,36}. Such polynomial chaos observables may be combined with the coarse-graining techniques presented here when no explicit coarse-scale descriptions of the particle system dynamics are available.

Appendix A

For Equation (29) with the initial condition

$$P_{XY}(x, y, t_0) = \delta(x)\delta(y),$$

(where t_0 is the blowup time) it is shown in the following that the solution is

$$P_{XY}(x, y, t) = \frac{\sqrt{3}}{\pi D^2(t-t_0)^2} e^{-\left(\frac{6(y-0.5x(t-t_0))^2}{D^2(t-t_0)^3} + \frac{x^2}{2D^2(t-t_0)}\right)}.$$

We can see that

$$\begin{aligned} \frac{\partial P_{XY}}{\partial t} &= e^{-\left(\frac{6(y-0.5x(t-t_0))^2}{D^2(t-t_0)^3} + \frac{x^2}{2D^2(t-t_0)}\right)} \\ &\cdot \left[\frac{-2\sqrt{3}}{\pi D^2(t-t_0)^3} + \frac{\sqrt{3}}{\pi D^2(t-t_0)^2} \left(\frac{(x-y)^2}{2D^2(t-t_0)^2} \right. \right. \\ &\left. \left. + \frac{18(y-0.5x(t-t_0))^2}{D^2(t-t_0)^4} + \frac{6(y-0.5x(t-t_0))x}{D^2(t-t_0)^3} \right) \right], \end{aligned}$$

$$\begin{aligned} x \frac{\partial P_{XY}}{\partial y} &= e^{-\left(\frac{6(y-0.5x(t-t_0))^2}{D^2(t-t_0)^3} + \frac{x^2}{2D^2(t-t_0)}\right)} \\ &\cdot \left[\frac{-\sqrt{3}x}{\pi D^2(t-t_0)^2} \cdot \frac{12(y-0.5x(t-t_0))}{D^2(t-t_0)^3} \right], \end{aligned}$$

$$\begin{aligned} \frac{D^2}{2} \frac{\partial^2 P_{XY}}{\partial x^2} &= \frac{D^2}{2} e^{-\left(\frac{6(y-0.5x(t-t_0))^2}{D^2(t-t_0)^3} + \frac{x^2}{2D^2(t-t_0)}\right)} \\ &\cdot \left[\frac{-4\sqrt{3}}{\pi D^2(t-t_0)^3} + \frac{\sqrt{3}}{\pi D^4(t-t_0)^4} \cdot \frac{(6(y)-4x(t-t_0))^2}{D^2(t-t_0)^2} \right]. \end{aligned}$$

Hence,

$$\frac{\partial P_{XY}}{\partial t} + x \frac{\partial P_{XY}}{\partial y} - \frac{D^2}{2} \frac{\partial^2 P_{XY}}{\partial x^2} = 0.$$

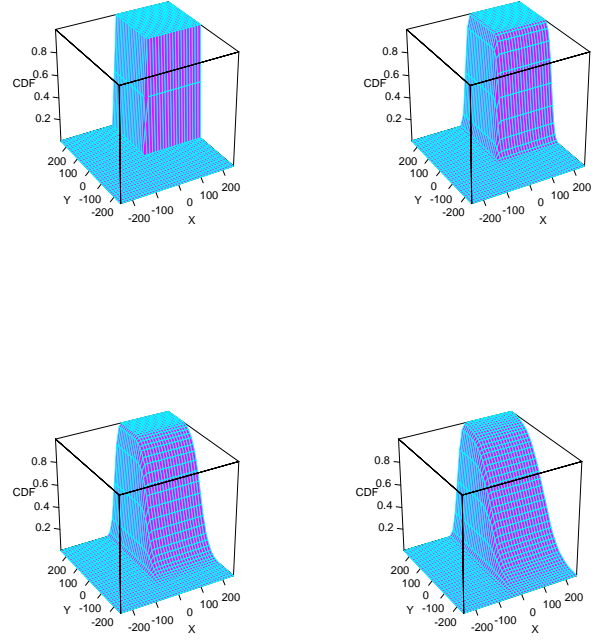


FIG. 4: True CDFs at a sequence of time steps; top left: $t = 0$, top right: $t = 300\Delta t$, bottom left: $t = 600\Delta t$, bottom right: $t = 900\Delta t$.

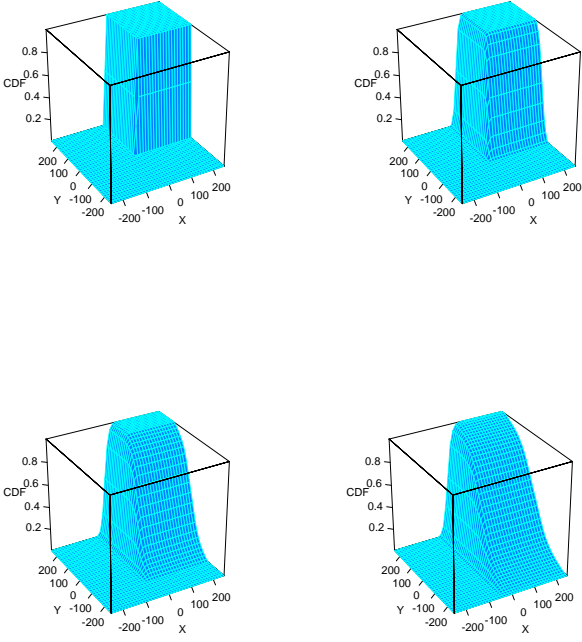


FIG. 5: CDFs at different time instances computed by the CPI method; top left: $t = 0$, top right: $t = 300\Delta t$, bottom left: $t = 600\Delta t$, bottom right: $t = 900\Delta t$.

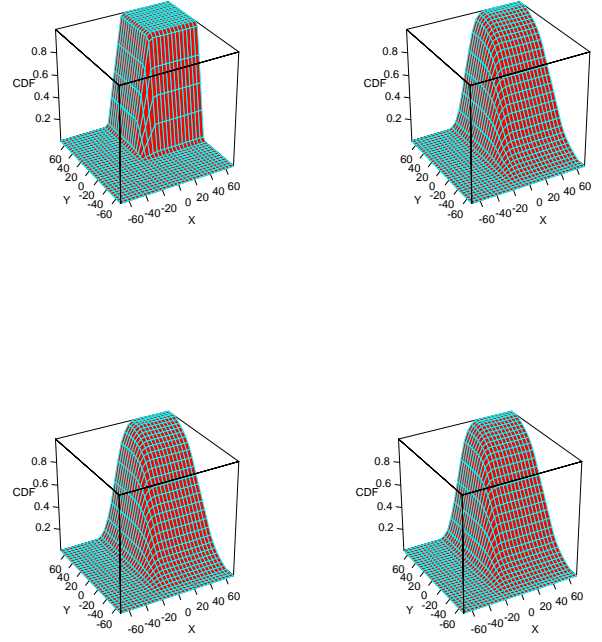


FIG. 7: Renormalized CDFs in Simulation 3; top left: initial CDF, top right: renormalized CDF after 2nd iteration, bottom left: renormalized CDF after 4th iteration, bottom right: renormalized CDF after 6th iteration.

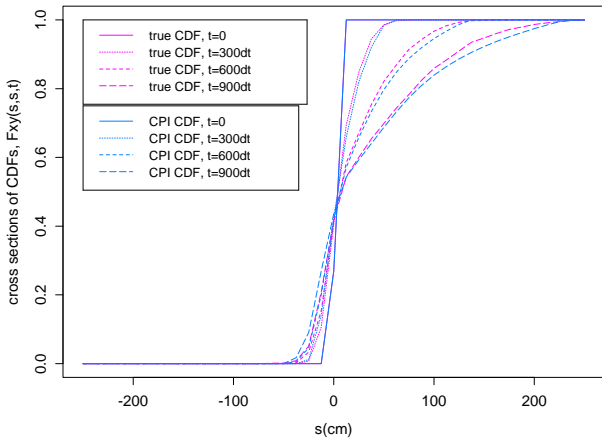


FIG. 6: Comparison between cross sections of true CDFs and CDFs computed by CPI.

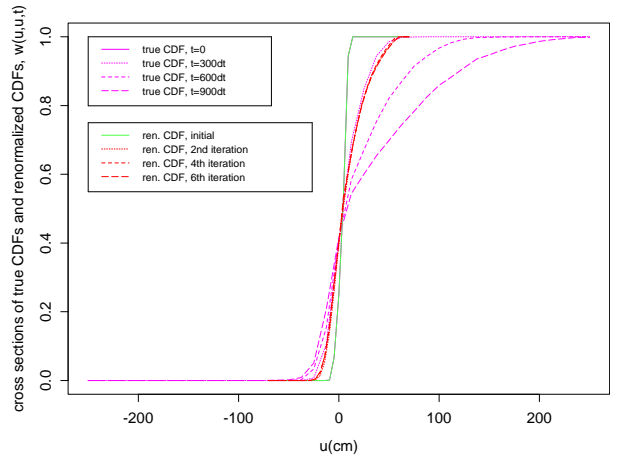


FIG. 8: Comparison between cross sections of true CDFs and rescaled CDFs in Simulation 3.

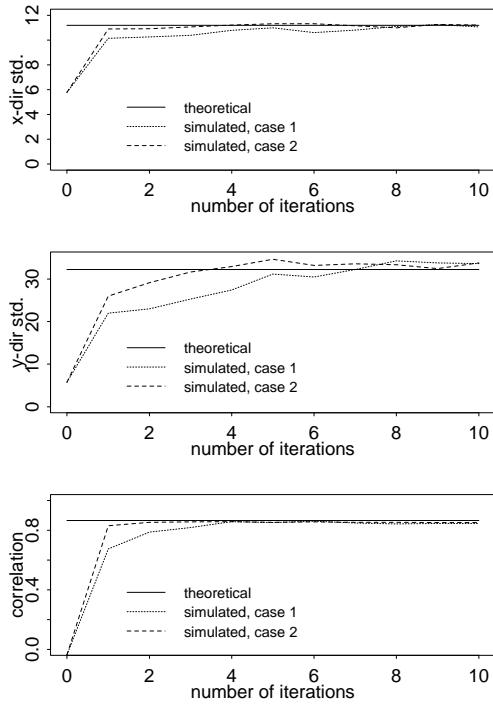


FIG. 9: Comparison for standard deviations and correlations of self-similar shapes in Simulation 3: Cases 1,2.

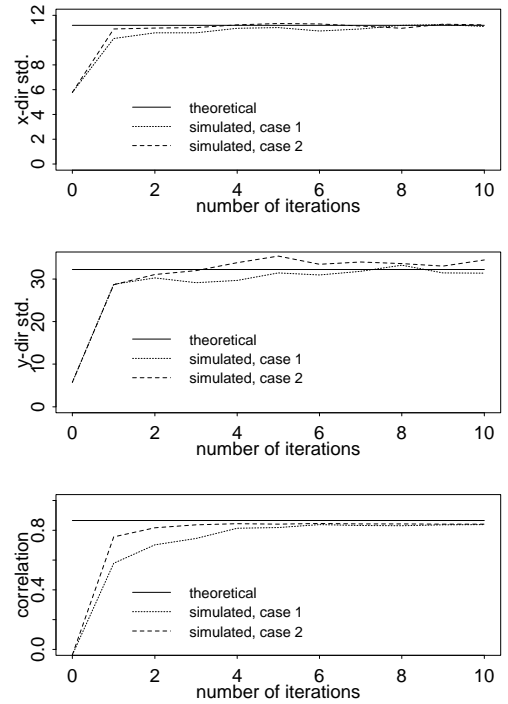


FIG. 11: Comparison for standard deviations and correlations of converged shapes in Simulation 4: Cases 1,2.

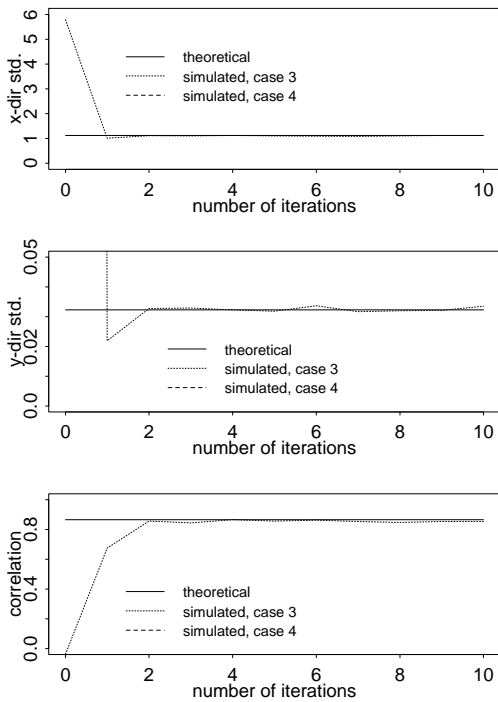


FIG. 10: Comparison for standard deviations and correlations of self-similar shapes in Simulation 3: Cases 3,4.

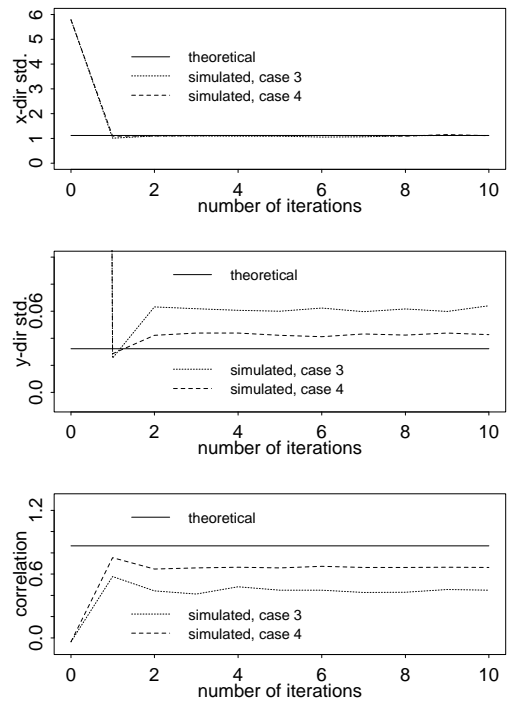


FIG. 12: Comparison for standard deviations and correlations of converged shapes in Simulation 4: Cases 3,4.

-
- [1] Kevrekidis, I.G.; Gear, C.W.; Hyman, J.M.; Kevrekidis, P.G.; Runborg, O.; Theodoropoulos, K. Equation-free coarse-grained multiscale computation: enabling microscopic simulators to perform system-level tasks, *Comm. Math. Sci.*, **2003**, 1(4), 715-762.
- [2] Kevrekidis, I.G.; Gear, C.W.; Hummer, G. Equation-free: the computer-assisted analysis of complex, multiscale systems, *A. I. Ch. Eng. Journal*, **2004**, 50(7), 1346-1354.
- [3] Gear, C.W. Projective Integration Methods for Distributions, *NEC Transaction*, **2001**, 130.
- [4] Setayeshgar, S.; Gear, C.W.; Othmer, H.G.; Kevrekidis, I.G. Application of Coarse Integration to Bacterial Chemotaxis, *SIAM Journal of Multiscale Modeling and Simulation*, **2005**, 4(1), 307-327.
- [5] Gear, C.W.; Kevrekidis, I.G.; Theodoropoulos, C. 'Coarse' Integration/Bifurcation Analysis via Microscopic Simulators: Micro-Galerkin Methods, *Computers and Chemical Engineering*, **2002**, 26, 941-963.
- [6] Faires, J.D.; Burden, R.L. *Numerical Methods*, PWS-Kent Pub. Co., Boston, 1993.
- [7] Gear, C.W.; Kevrekidis, I.G. Projective Methods for Stiff Differential Equations: Problems with Gaps in Their Eigenvalue Spectrum, *SIAM Journal of Scientific Computing*, **2002**, 24(4), 1091-1106.
- [8] Makeev, A.G.; Maroudas, D.; Kevrekidis, I.G. 'Coarse' stability and bifurcation analysis using stochastic simulators: Kinetic Monte Carlo examples, *Journal of Chemical Physics*, **2002**, 116, 10083-10091.
- [9] Siettos, C.I.; Graham, M.D.; Kevrekidis, I.G. Coarse Brownian Dynamics for Nematic Liquid Crystals: Bifurcation, Projective Integration, and Control via Stochastic Simulation, *Journal of Chemical Physics*, **2003**, 118(22), 10149-10156.
- [10] Theodoropoulos, C.; Sankaranarayanan, K.; Sundaresan, S.; Kevrekidis, I.G. Coarse Bifurcation Studies of Bubble Flow Lattice Boltzmann Simulations, *Chemical Engineering Science*, **2004**, 59, 2357-2362.
- [11] Runborg, O.; Theodoropoulos, C.; Kevrekidis, I.G. Effective bifurcation analysis: a time-stepper-based approach, *Nonlinearity*, **2002**, 15, 491-511.
- [12] Xiu, D.B.; Kevrekidis, I.G. Equation-free, multiscale computation for unsteady random diffusion, *SIAM Journal of Multiscale Modeling and Simulation*, **2004**, 4(3), 915-935.
- [13] Barenblatt, G.I. *Scaling, Self-Similarity and Intermediate Asymptotics*, Cambridge University Press, 1996.
- [14] Brandt, A.; Ron, D. Renormalization Multigrid (RMG): Statistically Optimal Renormalization Group Flow and Coarse-to-fine Monte Carlo Acceleration, *Journal of Statistical Physics*, **2001**, 102, 231-257.
- [15] Chorin, A.J. Conditional expectations and renormalization, *SIAM Journal of Multiscale Modeling and Simulation*, **2003**, 1, 105-118.
- [16] McLaughlin, D.W.; Papanicolaou, G.C.; Sulem, C.; Sulem, P.L. Focusing Singularity of the Nonlinear Schrödinger Equation, *Physics Review A*, **1986**, 34(2), 1200-1210.
- [17] LeMesurier, B.J.; Papanicolaou, G.C.; Sulem, C.; Sulem, P.L. "Focusing and Multifocusing solutions of the Nonlinear Schrödinger Equation. *Physica D*. **1988**. 31. 78-102.
- P.L. Local Structure of the self focusing singularity of the nonlinear Schrödinger Equation, *Physica D*, **1988**, 32, 210-226.
- [19] Chen, L.; Debenedetti, P.G.; Gear, C.W.; Kevrekidis, I.G. From molecular dynamics to coarse self-similar solutions: a simple example using equation-free computation, *JNNFM*, **2004**, 120, 215-223.
- [20] Rowley, C.W.; Marsden, J.E. Reconstruction Equations and the Karhunen-Loève expansion for systems with symmetry, *Physica D*, **2000**, 142, 1-19.
- [21] Aronson, D.G.; Betelu, S.T.; Kevrekidis, I.G. Going with the flow: a Lagrangian approach to self-similar dynamics and its consequences, <http://arxiv.org/abs/nlin/0111055>, **2001**
- [22] Siettos, C.I.; Kevrekidis, I.G.; Kevrekidis, P.G. Focusing revisited: a renormalization/bifurcation approach, *Nonlinearity*, **2003**, 16, 497-506.
- [23] Rowley, C.W.; Kevrekidis, I.G.; Marsden, J.E.; Lust, K. Reduction and reconstruction for self-similar dynamical systems, *Nonlinearity*, **2003**, 16, 1257-1275.
- [24] Zou, Y.; Kevrekidis, I.G.; Ghanem, R. Equation-free dynamic renormalization: Self-similarity in multidimensional particle system dynamics, *in press, Physical Review E*, **2005**.
- [25] Majda, A.J.; Kramer, P.R. Simplified models for turbulent diffusion: Theory, numerical modelling, and physical phenomena, *Physics Reports*, **1999**, 314, 237-574.
- [26] Abramowitz, M.; Stegun, I.A. *Handbook of Mathematical Functions*, Dover Publications, Inc., New York, 1970.
- [27] Li, J.; Liao, D.; Yip, S. Coupling continuum to molecular-dynamics simulation: Reflecting particle method and the field estimator, *Physical Review E*, **1998**, 57, 7259-7267.
- [28] Rico-Martinez, R.; Gear, C.W.; Kevrekidis, I.G. Coarse Projective KMC Integration: Forward/Reverse Initial and Boundary Value Problems, *Journal of Computational Physics*, **2004**, 196(2), 474-489.
- [29] Kelley, C.T. *Iterative Methods for Linear and Nonlinear Equations*, SIAM, 1995.
- [30] Panton, R.L. *Incompressible Flow*, New York: J. Wiley, 1996, 2nd ed.
- [31] Gihman, I.I.; Skorohod, A.V. *Stochastic Differential Equations*, Springer, 1972.
- [32] Milshtein, G.N. Approximate Integration of Stochastic Differential Equations, *Theory Prob. Application*, **1974**, 19, 557-562.
- [33] Okubo, A.; Karweit, M. Diffusion from a continuous source in a uniform shear flow, *Limn. and Oceano.*, **1969**, 14(4), 514-520.
- [34] Baptista, A.M.; Adams, E.E.; Gresho, P. Benchmarks for the transport equation: the convection-diffusion forum and beyond, *Quantitative Skill Assessment for Coastal Ocean Models (Edited by Lynch and Davies)*, AGU Coastal and Estuarine Studies, **1995**, 47, 241-268.
- [35] Ghanem, R. Probabilistic characterization of transport in heterogeneous media, *Computer Methods in Applied Mechanics and Engineering*, **1999**, 158, 199-220.
- [36] Xiu, D.B.; Karniadakis, G.E. A new stochastic approach to transient heat conduction modeling with uncertainty, *International Journal of Heat and Mass Transfer*, **2003**, 46, 4681-4693.